JGR Atmospheres

RESEARCH ARTICLE

10.1029/2020JD032677

Key Points:

- 2DVD observations of small drops high concentration in Meiyu precipitation are confirmed with polarimetric radar retrievals
- Warm rain processes are important pathways during the evolution of Meiyu convective precipitation in Eastern China
- Vertical structures of Meiyu convective and stratiform precipitation and their related DSD variations are identified

Correspondence to:

K. Zhao,
zhaokun@nju.edu.cn

Citation:

Wen, L., Zhao, K., Yang, Z., Chen, H., Huang, H., Chen, G., & Yang, Z. (2020). Microphysics of stratiform and convective precipitation during Meiyu season in Eastern China. *Journal of Geophysical Research: Atmospheres*, *125*, e2020JD032677. https://doi.org/10.1029/2020JD032677

Received 26 FEB 2020
Accepted 21 NOV 2020

Microphysics of Stratiform and Convective Precipitation During Meiyu Season in Eastern China

Long Wen[1,2,3], Kun Zhao[1,2], Zhonglin Yang[4], Haonan Chen[5], Hao Huang[1,2], Gang Chen[1,2], and Zhengwei Yang[1,2]

[1]Key Laboratory of Mesoscale Severe Weather/MOE and School of Atmospheric Sciences, Nanjing University, Nanjing, China, [2]State Key Laboratory of Severe Weather and Joint Center for Atmospheric Radar Research of CMA/NJU, Beijing, China, [3]Xichang Satellite Launch Center, Xichang, China, [4]CSIC PRIDe (Nanjing) Atmospheric and Oceanic Information System Co. Ltd, Nanjing, China, [5]Cooperative Institute for Research in the Atmosphere, Colorado State University, Fort Collins, CO, USA

Abstract The microphysical structure of Meiyu precipitation in Eastern China is investigated using two-dimensional video disdrometer (2DVD) and S-band polarimetric radar observations. The constrained-gamma raindrop size distribution (DSD) model derived from 2DVD observations performs well in representing Meiyu DSDs. The vertical variability of polarimetric variables and retrieved DSD parameters are then investigated. The results show different patterns of vertical behavior for convective and stratiform rain due to different ice-phase and precipitation microphysical processes. The radar reflectivity of stratiform rain presents a distinct bright band (with an average echo top between 6 and 7 km). In contrast, the convective rain shows a larger reflectivity with a relatively higher echo top at 8 km. Polarimetric signatures of convective rain above the 0°C isotherm imply the coexistence of rimed particles and aggregates, which is indispensable for the intense precipitation on the ground. However, with a bulk precipitation formed below the melting layer, warm rain processes are still critical pathways for the growth of raindrops and the subsequent generation of heavy rainfall. Furthermore, both convective and stratiform rain is dominated by raindrops <4 mm, and the increase in their rain intensity can mostly be attributed to the increase in raindrop concentration. The identified maritime nature of convective rain has a much higher (roughly more than two times) number concentration of raindrops than that of convection in a similar climate region. This study provides a more comprehensive picture of Meiyu precipitation microphysics in Eastern China.

1. Introduction

The accuracy of numerical model parameterization relies on a comprehensive understanding of the precipitation microphysical characteristics (Sun, 2005). As an important indicator of the precipitation microphysics, raindrop size distribution (DSD) is directly related to complex microphysical processes, such as accretion, collision–coalescence-breakup, and evaporation (Rosenfeld & Ulbrich, 2003). Therefore, knowledge of the temporal and spatial variations of DSD is critical for understanding the microphysical processes, improving quantitative precipitation estimation (QPE), and evaluating microphysics parameterization in model simulations (G. Zhang et al., 2006).

Precipitation microphysics can be characterized through joint disdrometer and polarimetric radar measurements (e.g., Bringi et al., 2003; Cao et al., 2008). As the disdrometer measurements are confined to a specific site at the surface, polarimetric radar parameters (i.e., differential reflectivity Z_{DR}, specific differential phase shift K_{DP}, and the correlation coefficient ρ_{hv}) can provide three-dimensional information on the bulk microphysical characteristics of precipitation over a wide area, such as the hydrometeor particle size, shape, and orientation (Doviak & Zrnić, 2006). With benefits from these microphysics-related parameters, researchers have attempted to estimate the three-dimensional distribution of normalized/constrained gamma DSDs (Ulbrich, 1983), which then helps to better reveal the evolution of precipitation microphysics (e.g., Bringi et al., 2009; Gorgucci et al., 2002; Vivekanandan et al., 2004; Zhang et al., 2001).

In East Asia, the quasi-stationary subtropical Meiyu front is a prominent feature during the summer monsoon season, which produces persistent heavy rainfall and severe flooding in East China, South Korea, and Japan (Ding & Chan, 2005). For disaster prevention and mitigation, precipitation microphysics of this

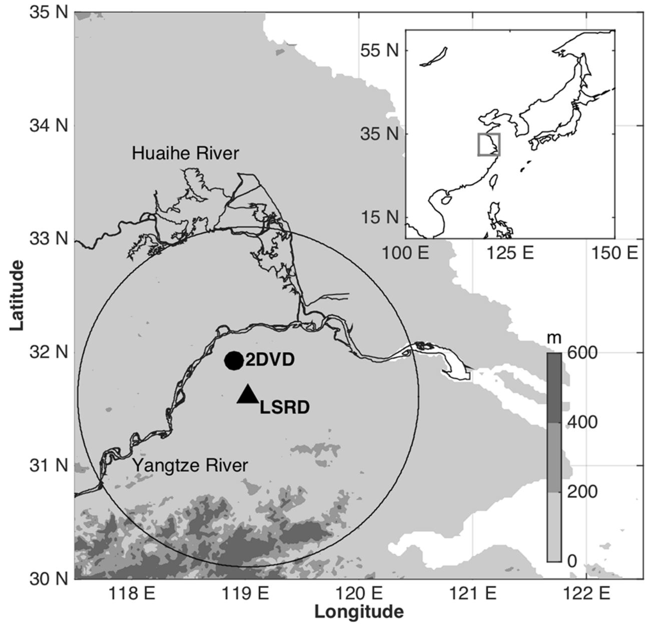

Figure 1. Field site locations of 2DVD and LSRD. Triangle denotes the location of LSRD radar and the dot marks the location of the 2DVD. The large solid circle indicates the 150-km observation radius of LSRD radar. The gray shading represents the terrain height. 2DVD, two-dimensional video disdrometer; LSRD, S-band polarimetric radar.

flooding and mudslide-produced Meiyu rainfall system have been the focus of many studies using observations from satellite, ground-based radar, and disdrometer (e.g., Luo et al., 2013; Oue et al., 2010; C.-Z. Zhang et al., 2006).

Results show that dominant convective cells are the primary contributors to the heavy Meiyu precipitation (Ninomiya & Shibagaki, 2007; Xu, 2013) in terms of accumulated rainfall amount (L. Wen et al., 2016). The typical meso-β-scale Meiyu convective cell has a median depth with a 15-dBZ echo top (reflectivity peak) lower than 8 km (4 km) through its lifetime (Shusse et al., 2009). Case studies concerning Meiyu precipitation microphysics in Okinawa, Japan, have been carried out in sequence by utilizing C-band polarimetric radar observations. Generally, Meiyu stratiform rain in Japan is composed of small raindrops with high concentration, and their averaged median volume diameter D_0 is about 1.55 mm (Oue et al., 2015; Shusse et al., 2009), while convection in the stratiform and convective rain zone is differentiated from the concentration of small (D_0 ∼1.2 mm) and large (D_0 ∼2 mm) raindrops (Oue et al., 2010, 2011). S-band polarimetric radar observations further reveal the vital role of warm rain processes in Meiyu convective rain in Taiwan (Chang et al., 2015), with weak updraft and high precipitation efficiency (over 50%).

However, the literature is limited to case studies and thus may be unpersuasive for a general insight view of Meiyu precipitation microphysics. Moreover, due to the dynamical nature of the precipitation system, along with land surface interactions and many other factors, Meiyu microphysics in Eastern China may differ from those documented in Japan and Taiwan. One evidence can be seen in L. Wen et al. (2016) based on 2-year two-dimensional video disdrometer (2DVD) observations, which show that Meiyu in Eastern China is characterized by a maritime nature, with higher raindrop concentration and smaller diameters than that in Japan and Taiwan (Bringi et al., 2006; Y. Chen, 2009). Recently, the microphysics of Meiyu extreme rainfall and convective events in Eastern China were investigated by Yang et al. (2019) and G. Chen et al. (2019). However, the statistical characteristics of near-surface DSD observed by disdrometers are not well confirmed, and the statistics in terms of the evolution and structure of Meiyu stratiform and convective precipitation have not yet been resolved in this particular region.

In this study, observations from an S-band polarimetric radar and a third-generation 2DVD during the 2013–2015 summer field campaigns of the Observation, Prediction, and Analysis of Severe Convection of China (OPACC; Xue, 2016) are utilized to (1) confirm our previous results (maritime nature of Meiyu convection in Eastern China) from ground-based 2DVD observations in L. Wen et al. (2016) and (2) further characterize the vertical structure of Meiyu precipitation and investigate the related microphysical processes correspondent to DSD characteristics near the ground. This study is useful to facilitate the understanding of Meiyu precipitation microphysics in Eastern China and ultimately produce more accurate radar QPE and model forecasts in this specific region.

2. Data and Methodology

The S-band polarimetric radar (hereafter referred to as LSRD) is located in Lishui (31.61°N, 119.03°E), southeast of Nanjing in Eastern China. The 2DVD is equipped at Jiangning site (JN; 31.93°N, 118.90°E), ∼37 km northwest to the LSRD. The temporal resolution of 2DVD and LSRD is 1 and 6 min, respectively. The locations of LSRD and 2DVD are marked in Figure 1. Note that raindrops with diameter <1, 1∼4, and >4 mm are considered small-, medium-, and large-size in this study. In situ sounding data at the JN site are collected twice a day as well. As indicated by the averaged sounding profile (with standard deviation) in Figure 2, south to southwesterly wind dominates all the time during the Meiyu season (from mid-June to mid-July) over the Yangtze-Huaihe River Basin. The southerly/southwesterly moist advection produces

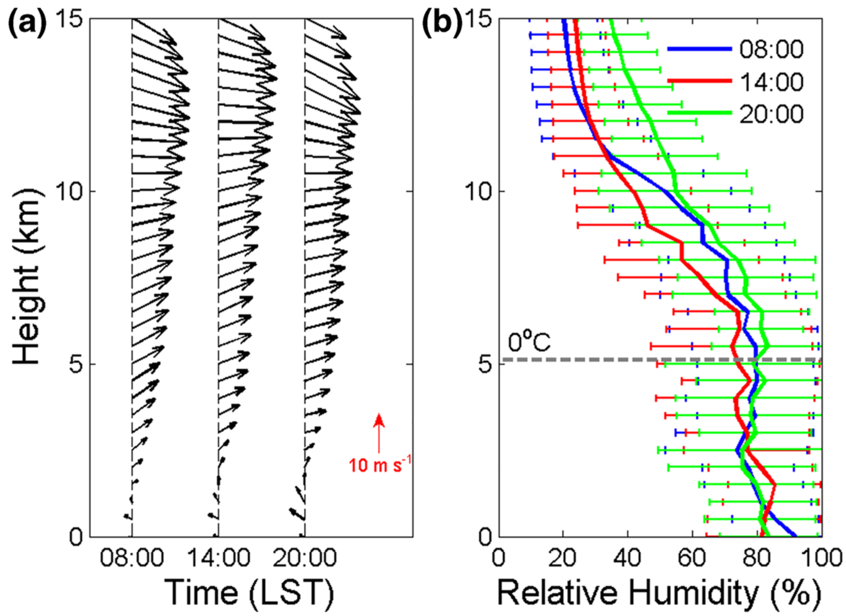

Figure 2. Profiles of (a) horizontal winds and (b) relative humidity observed by the sounding at 2DVD site from 2014 to 2015. 2DVD, two-dimensional video disdrometer.

a humid environment (although there are variations among different periods) that are favorable for heavy precipitation occurrence in this region.

2.1. Polarimetric Radar Data Processing

The LSRD operates in the volume coverage pattern (VCP-11) mode, with 14 elevations (from 0.5° to 19.5°). Its beam width and range resolution is 0.92° and 150 m, respectively. The polarimetric radar variables included here are radar reflectivity Z_H, Z_{DR}, K_{DP}, and ρ_{hv} during 2-year (2013 and 2014) LSRD observations covering nine Meiyu events (Table 1). Z_{DR} is determined by the shape of particles, while K_{DP} is related to the shape as well as the concentration of particles. Similar to WSR-88D, to maintain a 1-dB calibration precision for Z_H, an internally generated test signal is used for every volume scan to calibrate the reflectivity of LSRD. The non-meteorological echoes with $\rho_{hv} < 0.85$ are excluded (H. Chen et al., 2017). Although some useful data may be removed, the results of statistics should not be affected by this ρ_{hv} threshold. A five-gate median average (running mean) is performed to reduce the random fluctuations of Z_H (Z_{DR}). To correct the observed Z_{DR}, the Z_{DR} bias is estimated from the vertical pointing observation of raindrops below the melting level (2∼4 km) using the method developed by Gorgucci et al. (1999). The comparison suggests that the LSRD-corrected Z_{DR} agrees well with that derived from 2DVD measurements at disdrometer location with the differences within 0.2 dB (Wang et al., 2016). The calibrated Z_H and Z_{DR} satisfied the desired accuracy for further quantitative applications such as radar QPE and hydrometeor classification (Bringi & Chandrasekar, 2001).

Table 1
S-Band Polarimetric Dataset Used in This Study

No.	Dates (LST)	No. VCP 11 volumes scans
1	June 23, 2013	55
2	June 25, 2013	137
3	June 27, 2013	110
4	July 05, 2013	109
5	July 06–07, 2013	228
6	June 25, 2014	123
7	June 26, 2014	154
8	July 01–02, 2014	130
9	July 04–05, 2014	268

Abbreviation: VCP, volume coverage pattern.

After quality control, the Sorted Position Radar INTerpolation (SPRINT) software package from the National Center for Atmospheric Research (Mohr et al., 1986) is applied to interpolate the LSRD data onto a 1-km horizontally spaced and 0.5-km vertically spaced Cartesian grid. Then, 3-km height Constant-altitude position indicators (CAPPIs) data are used to identify convective and stratiform rain by the reflectivity texture described in Steiner et al. (1995). This classification is a robust separation algorithm by examining the sharpness and intensity of the radar reflectivity peaks. The peaks of radar reflectivity are regarded as the convective centers, and precipitation outside the convective region is stratiform. As mentioned in Steiner et al. (1995), this procedure would not underestimate the stratiform precipitation, and can accurately capture the essential precipitation climatology features. Hence, it is appropriate for the study of Meiyu statistics.

2.2. Disdrometer Data Processing

The third-generation 2DVD used in this study is a fast-scanning system. Its sample area is rectangular and approximately 10×10 cm^2. It is newly designed and thus the splashing and wind-induced errors are well mitigated and reduced (L. Wen et al., 2016). This instrument has been applied worldwide to achieve more accurate precipitation microphysics measurement (e.g., Bringi et al., 2003; Schönhuber et al., 2007; L. Wen et al., 2016). Since the horizontal and vertical grid resolution is close to 0.2 mm, the equivalent-volume diameters are sorted into 0.2 mm size categories, with the range of 0.1–8.1 mm (41 bins) in tabulated raindrop diameters. The 2DVD data used in this study are collected during the 2014 and 2015 Meiyu seasons. To minimize sampling error, only 1-min DSDs with drop counts larger than 50 are used. This gives 11,997 samples for further analysis.

Integral rain and DSD parameters are of interest in this study, i.e., the generalized intercept parameter (N_w, mm^{-1} m^{-3}), mass-weighted mean diameter (D_m, mm), liquid water content (LWC, g m^{-3}), and rain rate (R, mm h^{-1}) are all directly calculated from 2DVD-observed DSD. The standard deviation of the mass spectrum concerning D_m (σ_m, mm) can be directly computed from the nth-order weighted moment of the measured DSD and fall velocity. For comparison with LSRD observations, the polarimetric variables of Z_H (10log10(Z_h)) and Z_{DR} are also derived from 2DVD-observed DSDs using the T-matrix scattering technique (Vivekanandan et al., 1999; Waterman, 1965). Detailed expressions for the above-mentioned parameters can be found in L. Wen et al. (2016). Because the variation of S-band radar observables with temperature is negligible (Aydin & Giridhar, 1992), the temperature of the raindrop is set to 10°C. Moreover, the axis ratio proposed by Brandes et al. (2002) is adopted in this study.

2.3. Polarimetric Radar-Based DSD Retrieval

The constrained-gamma (C-G) method and the beta (β) method are most widely used in the literature for DSD retrieval. The β method retrieval is subject to high uncertainty mostly due to the K_{DP} noise (Anagnostou et al., 2008), while comparative analysis shows that DSD retrievals of the C-G method are more reasonable and closer to the disdrometer observations (Brandes et al., 2004a). The key of the C-G method is the empirical relationship between the two governing parameters of gamma DSD (the shape μ and slope Λ) with $N\left(D\right) = N_0 D^{\mu} \exp\left(-\Lambda D\right)$ (Zhang et al., 2001). As documented in G. Zhang et al. (2003), the μ–Λ relation reflects the actual physical DSD characteristic and thus is practical for the retrieval of DSD from radar observations.

In this study, the three governing parameters of gamma DSD, that is, the intercept parameter N_0 (mm$^{-1-\mu}$m^{-3}), μ (dimensionless), and Λ (mm^{-1}), are calculated from 2DVD observations using the sorting and averaging based on two parameters (SATP) method (Cao et al., 2008) and then the truncated moment fitting (TMF) method with the use of the second, fourth, and six moments of DSDs (Vivekanandan et al., 2004). For the SATP method, 2DVD-observed D_m and R are chosen to build a two-parameter grid to minimize error (see Figure 3a). Once the localized empirical μ–Λ relation is obtained from 2DVD observations, the three governing parameters of gamma DSD within the radar domain can be first retrieved from radar-observed Z_H and Z_{DR} following the C-G method (see details in Section 6.4 of G. Zhang, 2016), and then the other accompanied integral rain and DSD parameters can be directly calculated from the retrieved C-G DSD. The C-G method has been improved and generally proven to have good performance for DSD retrieval in Florida (Brandes et al., 2004a, 2004b; Vivekanandan et al., 2004; G. Zhang et al., 2006) and Oklahoma (Cao et al., 2008, 2010). Recently, polarimetric radar and 2DVD have been jointly employed in China for

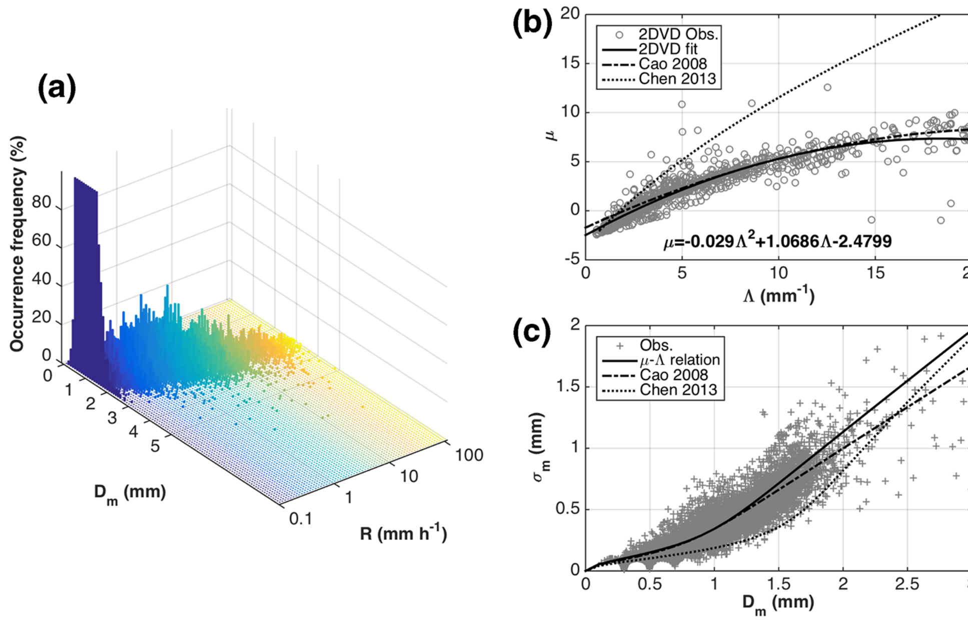

Figure 3. (a) Occurrence frequency of sorted DSD with respect to D_m (step is 0.05 mm) and R (step is 10%). (b) μ–Λ relations. The solid line represents a polynomial fit of 2DVD observations of Meiyu precipitation, and the dash–dotted line and the dotted line are the relationships obtained by Cao et al. (2008) and B. Chen et al. (2013), respectively. (c) Scatter plot of mass spectral width σ_m and D_m together with fitted curves. Crosses denote σ_m–D_m pairs calculated from observed DSDs. Solid, dot-dashed and dotted lines are the σ_m–D_m relations derived from the μ–Λ relations obtained in this study, by Cao et al. (2008) and B. Chen et al. (2013), respectively. 2DVD, two-dimensional video disdrometer; DSD, raindrop size distribution.

C-G model methodology validation (Liu et al., 2018) and precipitation microphysics investigation purposes (L. Wen et al., 2018).

3. Refined Constrained Gamma Model and Verification

3.1. Refined μ–Λ Relation and C-G Model

The derived μ–Λ relation shows variability across different seasons, climate regimes, and precipitation types (e.g., L. Wen et al., 2019; G. Zhang et al., 2003), and is susceptible to the data processing procedure as well as instrument error (L. Wen et al., 2019). In this study, 2DVD data are processed using the SATP and TMF methods to derive the statistical μ–Λ relation for Meiyu precipitation in Eastern China. As shown in Figure 3a, a large portion of samples (29.67%) with R smaller than 0.1 mm h^{-1} are present, which are usually composed of a high quantity of small drops. If the SATP method is not used, a large amount of small rain rate samples that contain large instrumental sampling error (G. Zhang et al., 2003) will dominate the procedure to fit the μ–Λ relation and thus produce significant bias. Therefore, the SATP data processing method, which balances the contribution of large and small rain rate samples by obtaining new DSD from each rain rate grid, is practical and necessary to reduce the statistical error of 2DVD observations. In Figure 3b, refined μ and Λ after data processing are fitted with a second-order polynomial to obtain the following statistical relation:

$$\mu = -0.029\Lambda^2 + 1.0686\Lambda - 2.4799 \quad (1)$$

For comparison, previously reported μ–Λ relations are included in Figure 3b as well. The μ–Λ relation in B. Chen et al. (2013) is derived using PARSIVEL disdrometer data for Meiyu convective rain in Nanjing. For most of the time, it has nearly 100% higher μ values compared with the 2DVD-derived relation for a given Λ. Such discrepancy can be partly attributed to the general underestimation (overestimation) of small (large) drops by PARSIVEL disdrometer (L. Wen et al., 2017). Another possible reason for the discrepancy could be the different data processing procedures used in B. Chen et al. (2013), in which a filter of R and the number of raindrops (instead of SATP procedure) are applied. Therefore, their relationship is limited to heavy precipitation with $\Lambda < 4\ \text{mm}^{-1}$. Using the same SATP method for 2DVD data, the μ–Λ relation newly derived in this study is very close to that in Oklahoma (Cao et al., 2008). The remaining minor differences between Cao et al. (2008) and our study may imply the natural variability of precipitation microphysics in these two climate regimes.

To verify the refined μ–Λ relation (Equation 1), we further compared the σ_m–D_m relation recalculated from the μ–Λ relation with those directly derived from observed DSDs. G. Zhang (2015) documented that a μ–Λ relation is essentially equivalent to a σ_m–D_m relation in representing the C-G DSD model. As shown in Figure 3c, the σ_m–D_m relation derived from B. Chen et al. (2013) based on PARSIVEL is generally biased to have a smaller σ_m (up to ~40%), while good agreement can be seen between the derived relation from the refined μ–Λ relation (Equation 1) and 2DVD observations. This suggests that the refined μ–Λ relation can represent Meiyu precipitation in Eastern China. Ultimately, the localized C-G model for Meiyu precipitation is obtained.

3.2. Verification of C-G Model

Observation of Meiyu event No. 9 (Table 1) is selected to verify the precision of C-G model retrieval. Figure 4 shows the LSRD-measured Z_H and Z_{DR} of this event at a 3-km height within a 100-km range, with convective rain area identified by the white contours identified by the Steiner et al. (1995) algorithm. As can be seen, the widespread stratiform rain area is usually embedded with medium- and small-sized convective cells, with relatively larger Z_H and Z_{DR} values (Figures 4a and 4b). A large Z_{DR} value can also be seen in the stratiform rain area. In general, the majority of Z_{DR} values are lower than 1.4 dB; this value corresponds to a retrieved D_m of ~1.75 mm. Moreover, Z_{DR} values for both precipitation types are generally lower than those observed in Japan (Shusse et al., 2009). These further confirmed the characterization of a smaller raindrop size but a higher concentration number of Meiyu precipitation in Eastern China than in Japan (L. Wen et al., 2016). Similar to typical meso-β-scale convective cells in C.-Z. Zhang et al. (2006), this Meiyu event also has a median depth with the echo top of 15 dBZ (reflectivity peak) lower than ~8 km (5 km) (Figure 4c). The Z_{DR} column coexists with the convective cells (Figure 4d). Detailed analysis of the vertical structure of Meiyu precipitation microphysics is provided in Section 4.

The evolution of 2DVD-observed DSDs during the mature stage of this Meiyu event (from 2000 to 2340 UTC) is presented (Figure 5). The observed DSDs are used to derive the polarimetric variables of Z_H and Z_{DR}, and then the DSD governing parameters are determined. Retrievals from the C-G model and a traditional exponential distribution (EXP; Marshall & Palmer, 1948) (when $\mu = 0$ in the Gamma model) model are given for comparison. As shown, the evolution of DSDs from stratiform (Figures 5a and 5b) to convective rain (Figures 5c–5i) and then the decaying period (Figures 5j–5l) are well characterized by the C-G model, while the EXP model shows large biases, especially at the small size end. The performance is consistent with G. Zhang et al. (2003) for the flexibility of the C-G model, especially for characterizing the instantaneous DSD variations in a wide range.

In Table 2, we further calculate the fraction bias of the estimated D_m, N_w, and R by using the C-G and EXP models, as well as the three-parameter gamma model fitted directly from the measured DSDs. As expected, the fractional error of N_w (D_m) from the C-G model is 6.29% (8.89%), which is much less than 18.9% (22.4%) from the EXP model but slightly larger than 1.35% (2.4%) from the directly fitted three-parameter gamma model. In the literature, retrieved results with a ~5% (15%) bias for D_m (N_t) are applicable for further rain microphysics studies in Oklahoma (Cao et al., 2008). Our localized C-G retrievals show comparable results, indicating better performance in representing DSD characteristics by the refined C-G model than the EXP ones. Hence, the C-G model is more applicable for further DSD retrieval of Meiyu precipitation in Eastern China.

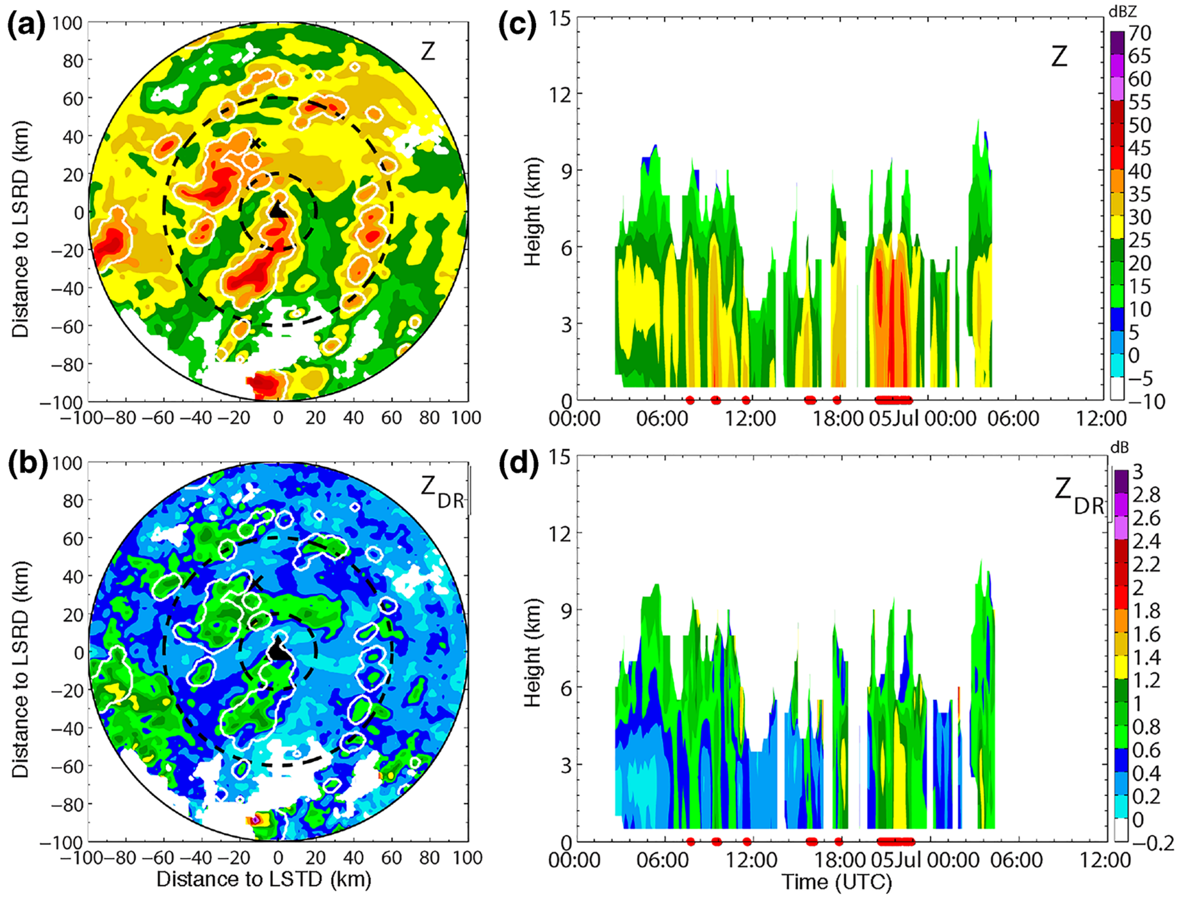

Figure 4. LSRD measured at 3-km height: (a) Z_H and (b) Z_{DR} on 0909 UTC, July 4, 2014, and the corresponding evolution of (c) Z_H and (d) Z_{DR} over the 2DVD site from 0000 UTC to 1200 UTC. The cross and filled triangles represent the locations of 2DVD and LSRD, and the white contours enclose the area of convective rain. Dashed circles delimitate the 20–60 km range of LSRD. 2DVD, two-dimensional video disdrometer; LSRD, S-band polarimetric radar.

3.3. Radar-Disdrometer Measurement Comparisons

Figure 6 shows the comparison of LSRD-measured radar variables (Z_H and Z_{DR}) and retrieved DSD parameters (utilizing C-G and EXP models) aloft the JN site with that directly calculated from 2DVD observations for the selected Meiyu event. In general, Z_H and Z_{DR} from LSRD at 0.5° elevation match the 2DVD observation well (Figures 6a and 6b), with the correlation coefficients (and RMSE) of 0.87 and 0.75 (3.2 dBZ and 0.25 dB), respectively. The discrepancies between LSRD and 2DVD measurements are mostly less than 2 dB (0.25 dB) for Z_H (Z_{DR}), except for a few brief periods (e.g., at 0900 UTC) that may result from inhomogeneity in the precipitation. These further demonstrated the reliability of the LSRD observations, which means that it is certainly adequate for subsequent analysis. For DSD retrievals, the overestimation of small drops with the EXP model results in significant overestimation of N_w and moderate underestimation of D_m, and subsequently an overestimation of R. Compared with the EXP model, the C-G model well improves the retrieval of D_m and also shows better retrieval of N_w and R. Considering the inconsistency of the sampling volume and measurement height between 2DVD and LSRD, we conclude that DSD retrieval from LSRD measurements using the localized C-G model (with the refined μ–Λ relation) is satisfactory and can represent the physical variations well.

Utilizing the localized C-G model, the DSD governing and integral parameters retrieved from LSRD at a 3-km height measurement of the Meiyu event at 0909 UTC (same as in Figure 4) are presented in Figure 7 (within 60 km radius). As seen, the stratiform rain showed up with $\log_{10}N_w$ lower than 4.6 and D_m between 1 and 1.4 mm, with LWC lower than 0.6 g m^{-3}. As a result, the stratiform R is typically <10 mm h^{-1}. The

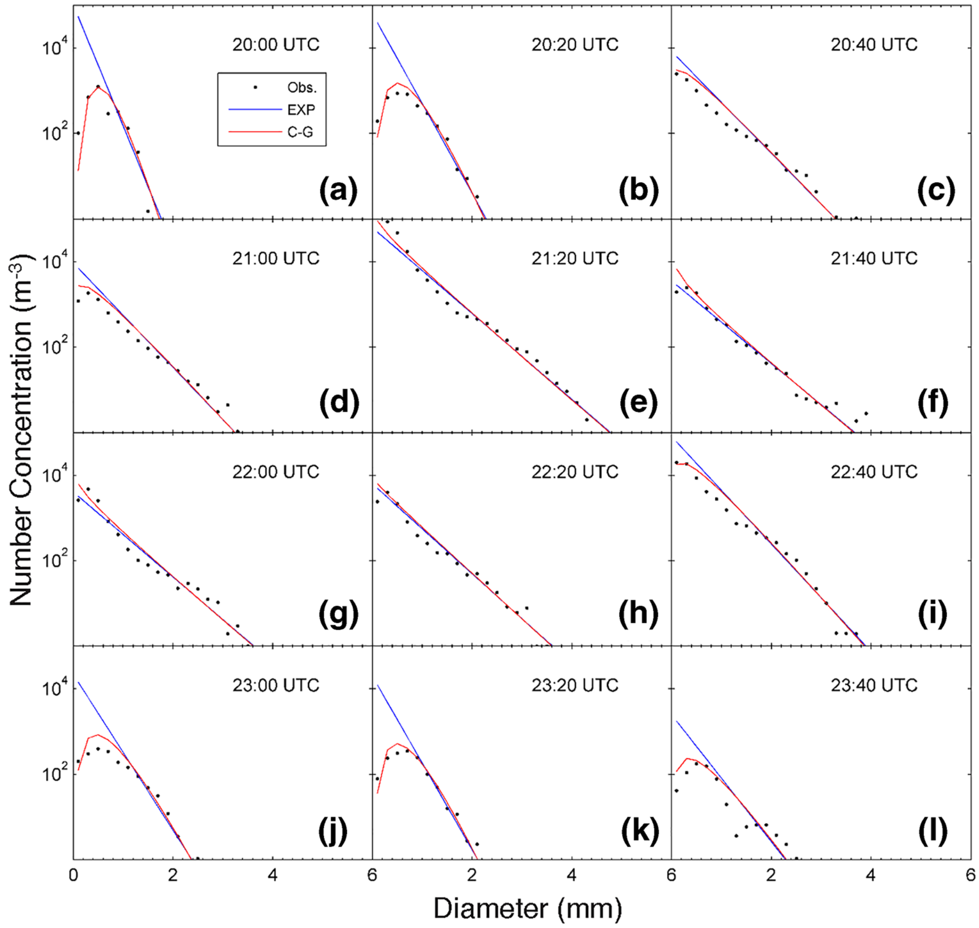

Figure 5. DSD evolution of the July 4, 2014 rain event at every 20 min time interval. Black dots are observed DSDs. Red lines and blue lines are fitted DSDs from Z_H and Z_{DR} using the C-G model and exponential distribution model, respectively. C-G, constrained-gamma; DSD, raindrop size distribution.

μ and Λ values are roughly around 2–6 and 4–12 mm^{-1}, respectively. In contrast, the estimated $\log_{10}N_w$ of embedded convective cells is much higher (typically >4.6), with D_m uniformly distributed between 1.2 and 1.4 mm and seldom exceeding 1.6 mm. Convective μ ranges from 0 to 2 and Λ varies from 2 to 5 mm^{-1}. Such parametric values suggest that the convective rain has a broader DSD. The LWC of convective cells is between 0.6 and 4 g m^{-3} while R ranges within 10–90 mm h^{-1}.

Generally, during this Meiyu event, D_m shows a more inhomogeneous distribution (mostly around 1–1.4 mm) than the other rainfall system occurred in this region, that is, squall line (G. Chen et al., 2019; J. Wen et al., 2017). On the contrary, the distribution of $\log_{10}N_w$ and LWC is highly relevant to Z_H variation (see Figure 4a). A higher Z_H value usually corresponds to a higher N_w and LWC, suggesting the major role of the increased number of small and medium-sized raindrops in increasing R.

Table 2
Bias and Fraction Error of DSD Physical Attributes Using Different Models

	Gamma	Exponential	C-G
$\text{Log}_{10}N_w$	0.0360	0.6433	0.1317
R	0.3359	1.5976	1.4608
D_m	−0.0267	−0.2239	−0.0508
$F(\log_{10}N_w)$	0.0135	0.1893	0.0629
$F(R)$	0.0373	0.3997	0.1709
$F(D_m)$	0.0240	0.2236	0.0889

Abbreviations: C-G, constrained-gamma; DSD, raindrop size distribution.

4. Statistical Rain Microphysics of Meiyu

With more polarization parameters, the 2-year LSRD dataset during the Meiyu season provides the first-ever opportunity to investigate the microphysical structure of Meiyu precipitation in Eastern China. Meanwhile, it is worth noting that the statistical results from radar, which can capture

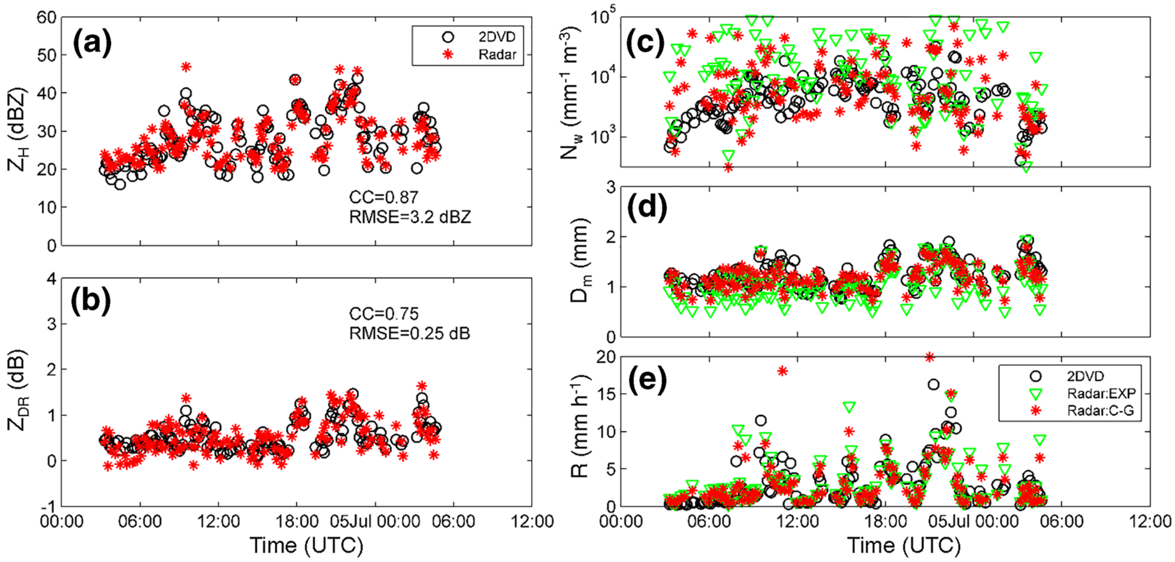

Figure 6. Comparison between radar and disdrometer data: (a) Z_H, (b) Z_{DR}, (c) N_w, (d) D_m, and (e) R. The radar scan elevation angle is 0.5°. The black circles represent 2DVD measurements while the green triangles and red asterisks represent radar-retrieval parameters using the exponential and C-G models, respectively. 2DVD, two-dimensional video disdrometer; C-G, constrained-gamma.

the evolution and spatial distribution of precipitation with a high temporal resolution, would be more representative than disdrometer measurements at a fixed site.

4.1. Vertical Structure of Meiyu Precipitation Microphysics

The stratiform and convective Z_H, Z_{DR}, and K_{DP} contoured frequencies by altitude diagrams (CFADs, Yuter & Houze, 1995) are presented to investigate the vertical microphysical structure of Meiyu precipitation (Figures 8a–8f). The modal (outlier) distribution of CFAD is referred to as frequencies greater (less) than 50% of the maximum frequency (Hence & Houze, 2011). To make sure that the top of the convective cells could be detected and the bin width is restricted within 1 km, only values within the 20–60 km radius of LSRD (between the two dashed circles in Figure 4a) are analyzed.

For stratiform rain, the modal distribution of Z_H is between 15 and 32 dBZ near the ground, with the maximum outlier not exceeding 38 dBZ (Figure 8a). The enhanced Z_H area is detected around a 5-km height (known as the bright band near 0°C isotherm). The melting level is roughly located at the top of the bright band. Compared with the stratiform rain, the modal distribution of Z_H for convective rain is narrower between 32 and 42 dBZ, and the outlier distribution seldom exceeding 48 dBZ (Figure 8d). The altitude of the 35-dBZ modal distribution is ~6 km, indicating the general formation of moderate Meiyu convection within warm clouds. Moreover, the modal distribution of 15-dBZ echo top height of convective rain is centered at the ~7–9 km level, implying moderate convection with a relative weak updraft. As documented in previous studies (Carr et al., 2017; Xu, 2013), the rapid decrease of Z_H with altitude above 0°C isotherm in warm rain events is an indicator of the limited amount of large frozen hydrometeors and/or supercooled water. A similar characteristic of Meiyu convection is shown in this study (Figure 8d).

The differences between stratiform and convective CFADs are visible for Z_{DR} and K_{DP}. The stratiform Z_{DR} below 0°C isotherm is small with its modal distribution around 0.1–0.6 dB (Figure 8b). The K_{DP} values of stratiform rain are also quite small (Figure 8c), suggesting limited LWC in stratiform rain. In contrast, with more water vapor transported to the upper level by updrafts in convective rain, raindrops aloft need a longer time for fallout and thus can grow larger while descending. As a result, the modal Z_{DR} is between 0.4 and 1 dB and the values of modal K_{DP} are relatively larger (Figures 8e and 8f). Above the melting layer, the different patterns of both Z_{DR} and K_{DP} for convective and stratiform rain should be attributed to different

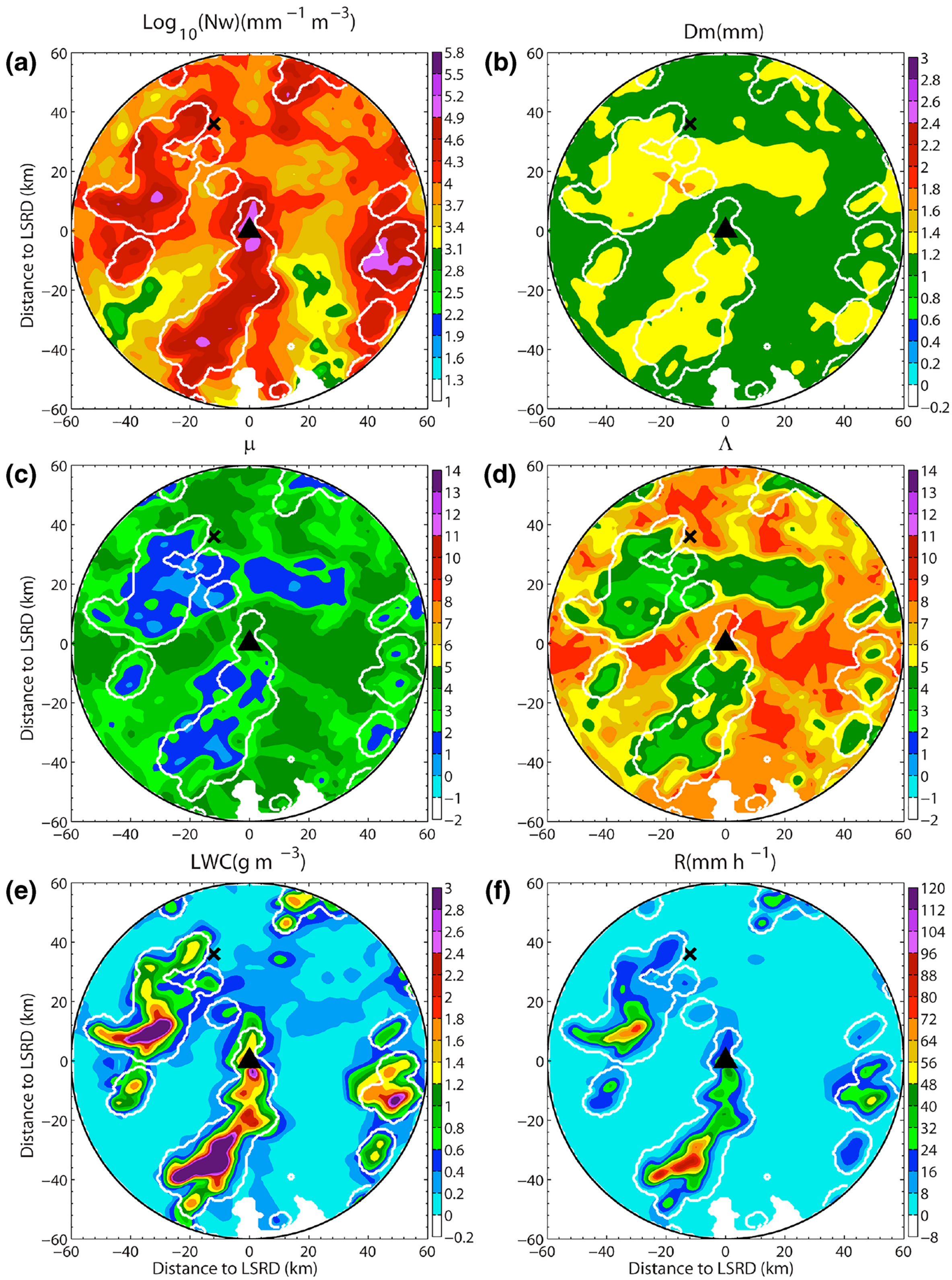

Figure 7. Contour plot of radar-retrieved (a) $\log_{10}N_w$, (b) D_m, (c) μ, (d) Λ, (e) LWC, and (f) R, from 3-km height measurement at 0909 UTC, July 4, 2014 within 60 km radius. The white contours enclose convective rain. LWC, Liquid water content.

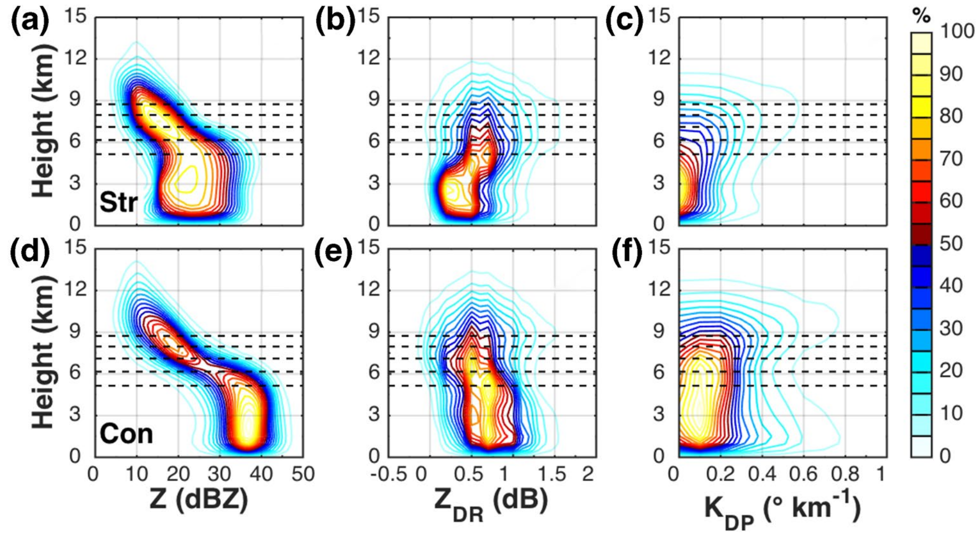

Figure 8. CFAD of stratiform and convective (a and d) Z_H, (b), (e) Z_{DR}, and (c), and (f) K_{DP} during Meiyu season. Data within radar range of 20–60 km are used. The horizontal black dashed lines from bottom to top, respectively, represent the level of 0°C, −5°C, −10°C, −15°C, and −20°C.

ice crystal microphysics at these altitudes. More compelling evidence is needed to better reveal the exact microphysical processes.

4.2. Evolution and Involved Microphysical Processes of Meiyu Precipitation

To better understand the vertical evolution and associated microphysical processes of Meiyu precipitation, the profiles of retrieved D_m and N_w are shown in Figure 9 with the merit of the C-G model. Note that, the water vapor condensation process will heat the lifted air parcels (the release of latent heat) to a higher temperature than the ambient air. Therefore, the melting layer in the precipitation system is slightly higher than the in situ sounding derived ambient 0°C isotherm level.

For stratiform rain above the melting layer, Z_H increases with decreasing height, while Z_{DR} and K_{DP} generally decrease. These characteristics are consistent with the preponderant aggregation and diffusional growth processes of ice particles in stratiform clouds (Houze, 1997; Penide et al., 2013; Yuter & Houze, 1995). Below the 0°C isotherm, there is a quasi-constant stratiform Z_H toward the ground, associated with a decrease (to

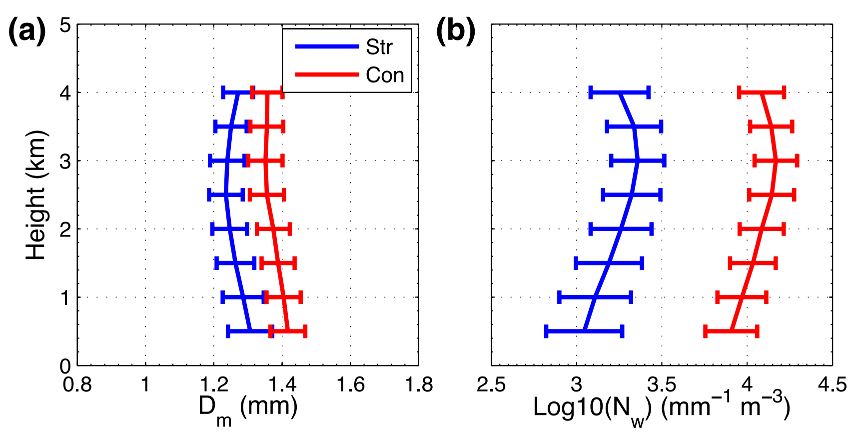

Figure 9. Profiles of radar-retrieved (a) D_m and (b) $\log_{10}N_w$ for stratiform (blue line) and convective (red line) precipitation during Meiyu season.

~3 km) and then increase (toward the ground) of Z_{DR} and K_{DP}. The corresponding stratiform LWC stays near-constant toward the ground (not shown). These signatures imply the combined effects of coalescence and breakup processes. While the coalescence process increases drop size and decreases number concentration, the breakup process does the opposite. These processes would change the drop spectrum that radar detected, and there can also be slight changes to the LWC due to the changes in the fall velocities. Moreover, since the environment is very humid below the melting level (Figure 2), the evaporation effect should be negligible. As further seen in retrieved DSD parameters (Figure 9), the stratiform D_m decreases while N_w increases from 4 to ~2.5 km. This could be explained that large drops coming from melting ice particles breakup to form a bunch of small drops. From a 2.5-km height toward the ground, the increase (decrease) of D_m (N_w) with a near-constant LWC is likely attributed to the overpowered coalescence than the breakup process.

In contrast, the convective rain exhibits a different pattern of vertical behavior. Above −10°C level, the increase of convective Z_H is associated with a decrease of Z_{DR} and K_{DP}. Note that graupel and hail have a small Z_{DR} due to random orientation (G. Zhang, 2016). The larger averaged convective Z_H but smaller Z_{DR} and K_{DP} than that of stratiform rain at these altitudes may imply the presence of rimed graupel and/or hail in convective rain. With the continued increase of convective Z_H, the mean Z_{DR} and K_{DP} also slightly increase. The melting of these particles is indispensable for heavy rainfall at the surface. However, warm rain processes are still vital pathways for the growth of raindrops and the eventual production of heavy rainfall, as also documented in previous precipitation microphysics studies for Meiyu cases (e.g., G. Chen et al., 2019).

The retrieved DSD parameters show that D_m stays near-constant (at ~1.36 mm) from a 4 to 3 km altitude while N_w slightly increases from 4.08 to 4.17 (Figure 9), suggesting that the rapid growth of convective LWC can be mostly attributed to the coalescence of raindrops and cloud droplets (autoconversion process to form drizzles). From 3 to 1 km, the D_m (N_w) starts to increase (decrease), while the LWC remains nearly constant ~0.48 g m^{-3}. These signatures suggest the dominant role of the coalescence process. The humid environment during the Meiyu season (Figure 2) ensures that this warm rain process occurs over a large depth. Furthermore, the mean convective D_m is only ~0.1 mm larger than stratiform D_m, but that of N_w is nearly eight times larger. The corresponding convective LWC is about four times larger than the stratiform ones. The discrepancies should be attributed to the competition of different microphysics processes involved in convective and stratiform rain as explained above.

Note that the mean liquid-layer Z_H, Z_{DR}, and K_{DP} values of Meiyu convective rain are consistent with the typical warm rain cases documented in Carr et al. (2017), which is characterized by Z_H values at ~35–40 dBZ, Z_{DR} ~ 0.5–1 dB, and K_{DP} ~ 0.1°–0.5° km^{-1}. The low Z_H but relatively high K_{DP} above the melting layer indicate a high concentration of small ice particles aloft. This implies that the contribution of ice-formed particles which melted into raindrops is relatively minor compared with classical continental storms with deep convection (e.g., G. Chen et al., 2019). Meanwhile, both convective and stratiform D_m vary within ±0.1 mm while descending toward the ground, suggesting that the intensification of Meiyu rainfall largely benefits from the increase in raindrop concentration through the warm rain process. This finding is consistent with the results from 2DVD observations (L. Wen et al., 2016).

4.3. The Frequency Distribution of DSD Parameters at 1 km Height

To further evaluate the statistical characteristics of Meiyu precipitation quantitatively, a joint frequency distribution in Z_H versus Z_{DR} and D_m versus $\log_{10}N_w$ space for stratiform and convective rain at 1 km height is presented (Figure 10). Note that the data are normalized by the maximum frequency in the dataset. As can be seen, the convective rain has much larger Z_H and slightly larger Z_{DR} than stratiform rain, with the peak frequency of Z_H and Z_{DR} for convective (stratiform) rain at ~37 (~24) dBZ and ~0.7 (~0.4) dB, respectively (black cross in each panel). When Z_H increases, the mean stratiform Z_{DR} varies between 0.4 and 0.9 dB with a maximum (over 5% frequency) at ~1.3 dB (Figure 10a). In contrast, the mean convective Z_{DR} increases from ~0.6 to 1.35 dB (with a maximum ~1.6 dB) with the increase of Z_H from 20 dBZ to a maximum at ~48 dBZ (Figure 10b). Generally, Z_{DR} seldom exceeds 1.5 dB for both the two types of rain, indicating the dominance of small- and medium-sized raindrops in Meiyu precipitation.

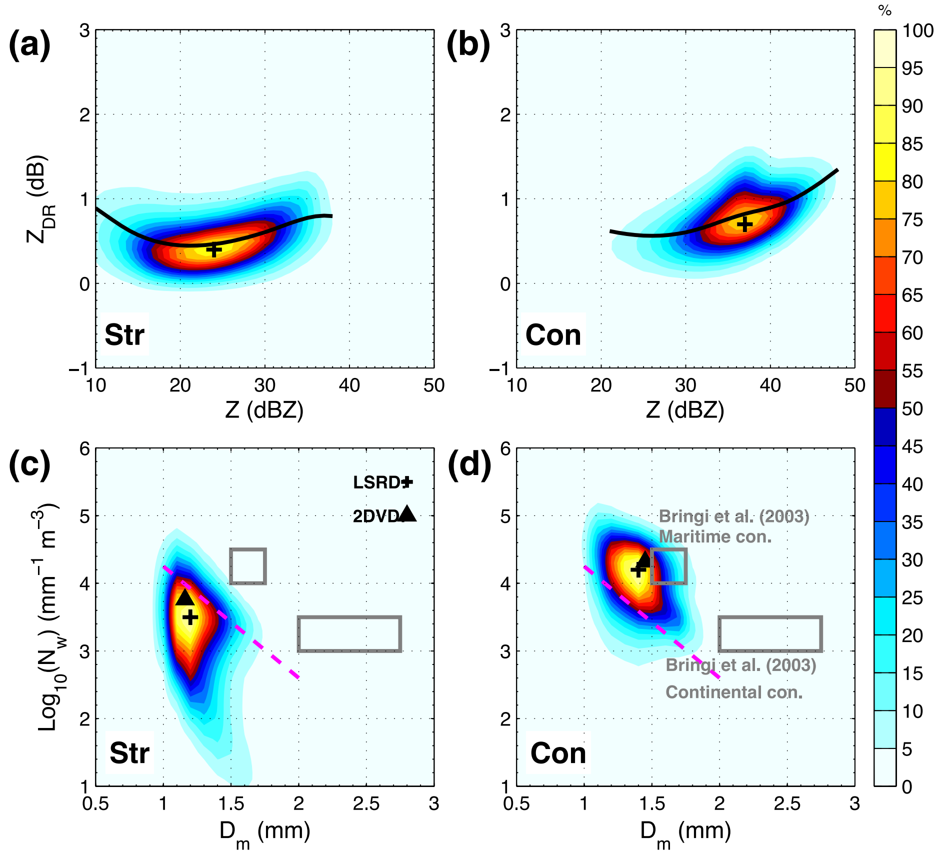

Figure 10. Frequency distributions of Z_H versus Z_{DR} for (a) stratiform rain, (b) convective rain at 1 km during Meiyu season, and (c and d) the corresponding frequency distribution of radar-retrieved $\log_{10}N_w$ and D_m. The distribution is normalized by the maximum frequency in the dataset.

As seen in Figure 10c, Meiyu stratiform D_m–$\log_{10}N_w$ pairs are plotted over a wide range, with the majority of them located to the left of the stratiform line in Bringi et al. (2003). As suggested by Bringi et al. (2003), the large variation of stratiform rain D_m–$\log_{10}N_w$ pairs is consistent with the different microphysical processes, that is, the melting of snowflakes to form a larger D_m but lower N_w, and/or the melting of rimed particles or tiny graupel to form a smaller D_m but higher N_w. The averaged value of D_m ~1.2 mm and $\log_{10}N_w$ ~3.5 ($\log_{10}$ $\mathrm{mm^{-1}\ m^{-3}}$) suggests that aggregates/snowflakes contribute most to Meiyu stratiform precipitation, similar to that in Japan (Oue et al., 2015). Note that the two gray rectangles in Figure 10d correspond to the two identified clusters (maritime-like and continental-like convective) in Bringi et al. (2003). The D_m–$\log_{10}N_w$ pairs of convective rain are mostly plotted close to the maritime cluster and barely appear in the continental ones, with the averaged D_m and $\log_{10}N_w$ value at ~1.4 and 4.2 mm, indicating a maritime nature of Meiyu convective rain in Eastern China. The LSRD retrieved characterization of Meiyu precipitation agrees well with 2-year 2DVD observations in L. Wen et al. (2016, 2017), which showed a mean D_m and $\log_{10}N_w$ value of 1.45 and 4.32 mm, respectively (triangles in Figures 10c and 10d).

The occurrence frequencies of retrieved D_m, $\log_{10}N_w$, and R are further presented to resolve the DSD variability of stratiform and convective rain (Figure 11). The first noteworthy character is that both stratiform and convective rain have a small width of D_m that varies approximately from ~0.9 to ~1.9 mm, with the frequency of convective D_m relatively higher when $D_m > 1.3$ mm (Figure 11a). The relatively larger convective D_m is likely related to the enhanced ice microphysics via the activation of the riming process in moderate Meiyu convection. In contrast, the convective N_w shows a narrower distribution and a much higher frequency for $N_w > 3.7$ (Figure 11b). This means that the stratiform and convective rain is mainly differentiated on raindrop concentration rather than drop diameter. Because of the significantly higher amount of small- and

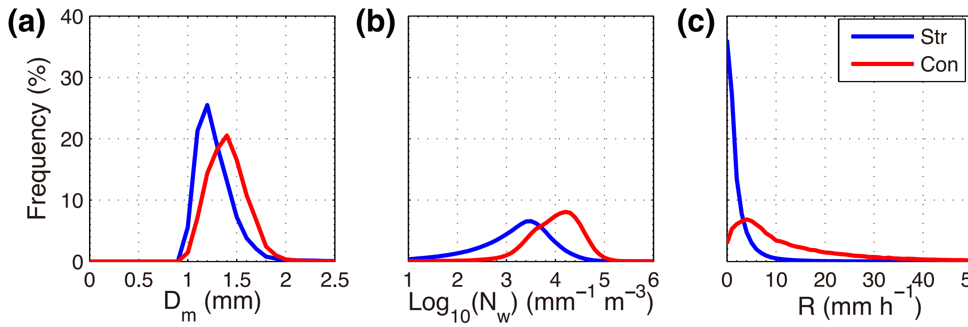

Figure 11. The occurrence frequencies of (a) D_m, (b) $\log_{10}N_w$, and (c) R for stratiform and convective precipitation at 1-km above sea level (ASL).

medium-sized raindrops, the corresponding convective R shows a much higher frequency for $R > 5$ mm h^{-1} while the stratiform R seldom exceeds 10 mm h^{-1} (Figure 11c).

Figure 12 shows the frequency distributions of D_m and N_w versus R with different rain types. For the stratiform rain, D_m decreases slightly toward ~1.2 mm while N_w increases rapidly (more than an order of magnitude) with the enhancement of rain intensity (Figures 12a and 12c). The convective D_m converges to a constant value at ~1.5 mm, while N_w increases with the increase of R through more efficient collision–coalescence-breakup mechanisms. The frequency distributions of these three parameters (D_m, $\log_{10}N_w$, and R) with respect to 15-dBZ echo top heights are further given in Figure 13. The modal distribution of stratiform rain is between 6 and 7 km with a 5% maximum height lower than 9 km. The convective rain shows a relatively higher echo top with the modal distribution between 6 and 8 km (and the outlier not exceeding 10.5-km height), corresponding to moderate convection with a relative weak updraft. Hence, warm rain processes play a vital role in the formation and evolution of both stratiform and convective Meiyu precipitation in Eastern China. Along with the increase of R, the echo top increases slightly during low rain rates and then stays near constant at ~7–8 km height because of the weak updraft. The similar echo top height

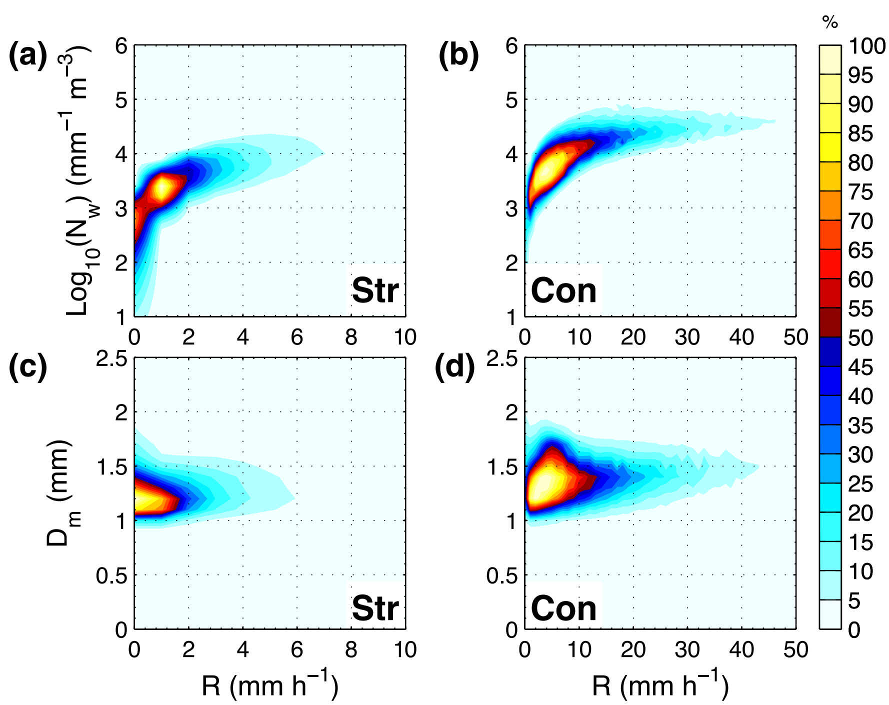

Figure 12. Frequency distributions of (a), (b) $\log_{10}N_w$ and (c), (d) D_m versus R at 1 km ASL for stratiform (left) and convective (right) precipitation.

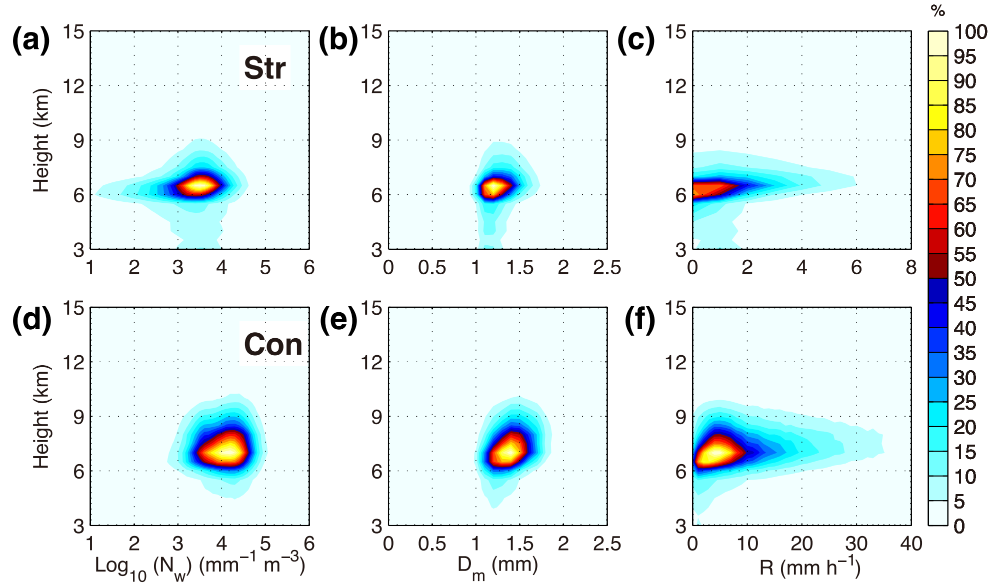

Figure 13. Frequency distributions of $\log_{10}N_w$ (left), D_m (middle), and R (right) with respect to 15-dBZ echo top height for (a–c) stratiform and (d–f) convective precipitation.

during heavy rainfall implies a homogeneous cloud and subsequent precipitation microphysics. Under this homogeneous condition, precipitation DSDs may easily reach the equilibrium state. With a constant D_m, the enhancement of R is mainly resulted from the increase in raindrop concentration, as is evident in the aforementioned analysis (see Figure 12).

5. Conclusion

In this study, 2-year joint observations from a 2DVD and an S-band polarimetric radar are used to reveal precipitation microphysics during the Meiyu season in Eastern China. The major conclusions of this study are summarized as follows:

1. Comparative analysis shows that the evolution of DSDs from stratiform to convective rain and the subsequent decaying period are well characterized by the C-G model with refined μ–Λ relation from 2DVD observations, suggesting that the localized C-G model gives satisfactory retrieval results and maintains the physical variations well for Meiyu precipitation
2. Meiyu convective and stratiform rain presents different patterns of vertical behavior due to the competition of different microphysical processes. Warm rain processes dominate the evolution of Meiyu convective rainfall, with the mean liquid-layer convective Z_H, Z_{DR}, and K_{DP} values consistent with typical warm rain cases in Carr et al. (2017). Below the 0°C isotherm, the mean retrieved convective D_m is only ~0.1 mm larger than stratiform D_m, but that of N_w is nearly eight times larger. Hence, the rapid growth of convective LWC should be attributed more to the increase in the number concentration of raindrops through the enhanced warm rain processes in a humid environment
3. The retrieved convective D_m–$\log_{10}N_w$ pairs at 1 km height are mostly plotted close to the maritime cluster, indicating a maritime nature of Meiyu convective rain in Eastern China. This agrees well with 2-year 2DVD observations in L. Wen et al. (2016), with a much higher concentration of small- and medium-size drops than Meiyu/Baiu in the similar climate regimes of Japan and Taiwan. The similar moderate echo top height (7–8 km) of Meiyu convective rain implies a homogeneous cloud and subsequent precipitation microphysics, under which the rain DSDs reach the equilibrium state with a constant D_m, as previously documented in L. Wen et al. (2016)

In this study, a comprehensive picture of Meiyu precipitation microphysics is provided based on long-term polarimetric radar observations in Eastern China. The refined C-G model is also applicable to develop algorithms in improving QPE for satellite and ground radar observations. To accurately simulate precipitation systems, more efforts are still needed to apply polarimetric radar data in numerical model validation, initiation, and assimilation.

Data Availability Statement

The field campaign data used in this study are available at https://doi.org/10.5281/zenodo.3978822.

Acknowledgments
This work was supported jointly by the National Key Research and Development Program of China (Grant No. 2017YFC1501703), the National Natural Science Foundation of China (Grant Nos 42025501, 41875053, 41675023, 41805015, and 41905021), the 5th "333 High-level Personnel Training Project" of Jiangsu Province (BRA2019037), the Science and Technology Project of Zhejiang Province (grant 2017C03035), and the Open Research Program of the State Key Laboratory of Severe Weather (2020LASW-A01). Observational data used in this study were collected by the field campaign of a National 973 Project (2013CB430101). The authors acknowledge Dr. Guifu Zhang for the constructive suggestions that improved this manuscript. They also thank Dr. Su Liu for his valuable work on data collection and processing.

References

Anagnostou, M. N., Anagnostou, E. N., Vulpiani, G., Montopoli, M., Marzano, F. S., & Vivekanandan, J. (2008). Evaluation of X-band polarimetric-radar estimates of drop-size distributions from coincident S-band polarimetric estimates and measured raindrop spectra. *IEEE Transactions on Geoscience and Remote Sensing*, *46*(10), 3067–3075.

Aydin, K., & Giridhar, V. (1992). C-band dual-polarization radar observables in rain. *Journal of Atmospheric and Oceanic Technology*, *9*(4), 383–390.

Brandes, E. A., Zhang, G., & Vivekanandan, J. (2002). Experiments in rainfall estimation with a polarimetric radar in a subtropical environment. *Journal of Applied Meteorology*, *41*(6), 674–685.

Brandes, E. A., Zhang, G., & Vivekanandan, J. (2004a). Comparison of polarimetric radar drop size distribution retrieval algorithms. *Journal of Atmospheric and Oceanic Technology*, *21*(4), 584–598.

Brandes, E. A., Zhang, G., & Vivekanandan, J. (2004b). Drop size distribution retrieval with polarimetric radar: Model and application. *Journal of Applied Meteorology*, *43*(3), 461–475.

Bringi, V., & Chandrasekar, V. (2001). *Polarimetric Doppler weather radar: Principles and applications*. Cambridge, UK: Cambridge University Press.

Bringi, V., Chandrasekar, V., Hubbert, J., Gorgucci, E., Randeu, W. L., & Schoenhuber, M. (2003). Raindrop size distribution in different climatic regimes from disdrometer and dual-polarized radar analysis. *Journal of the Atmospheric Sciences*, *60*(2), 354–365.

Bringi, V., Thurai, M., Nakagawa, K., Huang, G., Kobayashi, T., Adachi, A., et al. (2006). Rainfall estimation from C-band polarimetric radar in Okinawa, Japan: Comparisons with 2D-video disdrometer and 400MHz wind profiler. *Journal of the Meteorological Society of Japan*, *84*(4), 705–724.

Bringi, V., Williams, C., Thurai, M., & May, P. (2009). Using dual-polarized radar and dual-frequency profiler for DSD characterization: A case study from Darwin, Australia. *Journal of Atmospheric and Oceanic Technology*, *26*(10), 2107–2122.

Cao, Q., Zhang, G., Brandes, E., & Schuur, T. (2010). Polarimetric radar rain estimation through retrieval of drop size distribution using a Bayesian approach. *Journal of Applied Meteorology and Climatology*, *49*(5), 973–990.

Cao, Q., Zhang, G., Brandes, E., Schuur, T., Ryzhkov, A., & Ikeda, K. (2008). Analysis of video disdrometer and polarimetric radar data to characterize rain microphysics in Oklahoma. *Journal of Applied Meteorology and Climatology*, *47*(8), 2238–2255. https://doi.org/10.1175/2008JAMC1732.1

Carr, N., Kirstetter, P. E., Gourley, J. J., & Hong, Y. (2017). Polarimetric signatures of midlatitude warm-rain precipitation events. *Journal of Applied Meteorology and Climatology*, *56*(3), 697–711.

Chang, W.-Y., Lee, W.-C., & Liou, Y.-C. (2015). The kinematic and microphysical characteristics and associated precipitation efficiency of subtropical convection during SoWMEX/TiMREX. *Monthly Weather Review*, *143*(1), 317–340.

Chen, Y. (2009). *The characteristic of drop size distribution during SoWMEX (in Chinese)*. (MS thesis, p. 68). Chungli, Taiwan: Institute of Atmospheric Physics, National Central University. http://ir.lib.ncu.edu.tw/handle/987654321/5063

Chen, H., Chandrasekar, V., & Bechini, R. (2017). An improved dual-polarization radar rainfall algorithm (DROPS2.0): Application in NASA IFloodS field campaign. *Journal of Hydrometeorology*, *18*(4), 917–937.

Chen, B., Yang, J., & Pu, J. (2013). Statistical characteristics of raindrop size distribution in the Meiyu season observed in Eastern China. *Journal of the Meteorological Society of Japan*, *91*(2), 215–227.

Chen, G., Zhao, K., Wen, L., Wang, M., Huang, H., Wang, M., et al. (2019). Microphysical characteristics of three convective events with intense rainfall observed by polarimetric radar and disdrometer in Eastern China. *Remote Sensing*, *17*(11), 2004.

Ding, Y., & Chan, J. C. (2005). The East Asian summer monsoon: An overview. *Meteorology and Atmospheric Physics*, *89*(1–4), 117–142.

Doviak, R. J., & Zrnić, D. S. (2006). *Doppler radar and weather observations* (2nd ed.), New York, NY: Dover Publications.

Gorgucci, E., Chandrasekar, V., Bringi, V. N., & Scarchilli, G. (2002). Estimation of raindrop size distribution parameters from polarimetric radar measurements. *Journal of the Atmospheric Sciences*, *59*(15), 2373–2384.

Gorgucci, E., Scarchilli, G., & Chandrasekar, V. (1999). A procedure to calibrate multiparameter weather radar using properties of the rain medium. *IEEE Transactions on Geoscience and Remote Sensing*, *37*(1), 269–276.

Hence, D. A., & Houze, R. A., Jr (2011). Vertical structure of hurricane eyewalls as seen by the TRMM Precipitation Radar. *Journal of the Atmospheric Sciences*, *68*(8), 1637–1652.

Houze, R., Jr (1997). Stratiform precipitation in regions of convection: A meteorological paradox? *Bulletin of the American Meteorological Society*, *78*(10), 2179–2196.

Liu, X., Wan, Q., Wang, H., Xiao, H., Zhang, Y., Zheng, T., & Feng, L. (2018). Raindrop size distribution parameters retrieved from Guangzhou S-band polarimetric radar observations. *Journal of Meteorological Research*, *32*(4), 571–583. https://doi.org/10.1007/s13351-018-7152-4

Luo, Y., Wang, H., Zhang, R., Qian, W., & Luo, Z. (2013). Comparison of rainfall characteristics and convective properties of monsoon precipitation systems over South China and the Yangtze and Huai River Basin. *Journal of Climate*, *26*(1), 110–132.

Marshall, J. S., & Palmer, W. M. (1948). The distribution of raindrops with size. *Journal of Meteorology*, *5*(4), 165–166.

Mohr, C. G., Jay Miller, L., Vaughan, R. L., & Frank, H. W. (1986). The merger of mesoscale datasets into a common Cartesian format for efficient and systematic analyses. *Journal of Atmospheric and Oceanic Technology*, *3*(1), 143–161.

Ninomiya, K., & Shibagaki, Y. (2007). Multi-scale features of the Meiyu-Baiu front and associated precipitation systems. *Journal of the Meteorological Society of Japan*, *85*, 103–122.

Oue, M., Ohigashi, T., Tsuboki, K., & Nakakita, E. (2015). Vertical distribution of precipitation particles in Baiu frontal stratiform intense rainfall around Okinawa Island, Japan. *Journal of Geophysical Research: Atmospheres*, *120*(11), 5622–5637. https://doi.org/10.1002/2014JD022712

Oue, M., Uyeda, H., & Lee, D. I. (2011). Raindrop size distribution parameters estimated from polarimetric radar variables in convective cells around Okinawa Island during the Baiu period. *Asia-Pacific Journal of Atmospheric Sciences*, *47*(1), 33–44.

Oue, M., Uyeda, H., & Shusse, Y. (2010). Two types of precipitation particle distribution in convective cells accompanying a Baiu frontal rainband around Okinawa Island, Japan. *Journal of Geophysical Research*, *115*(D2), D02201. https://doi.org/10.1029/2009JD011957

Penide, G., Kumar, V. V., Protat, A., & May, P. T. (2013). Statistics of drop size distribution parameters and rain rates for stratiform and convective precipitation during the North Australian wet season. *Monthly Weather Review*, *141*(9), 3222–3237.

Rosenfeld, D., & Ulbrich, C. W. (2003). Cloud microphysical properties, processes, and rainfall estimation opportunities. In *Radar and Atmospheric Science: A Collection of Essays in Honor of David Atlas, Meteorological Monographs* (pp. 237–258). Boston, MA: American Meteorological Society. https://doi.org/10.1007/978-1-878220-36-3_10

Schönhuber, M., Lammer, G., & Randeu, W. (2007). One decade of imaging precipitation measurement by 2D-video-distrometer. *Advances in Geosciences*, *10*(10), 85–90.

Shusse, Y., Nakagawa, K., Takahashi, N., Satoh, S., & Iguchi, T. (2009). Characteristics of polarimetric radar variables in three types of rainfalls in a Baiu front event over the East China Sea. *Journal of the Meteorological Society of Japan*, *87*(5), 865–875.

Steiner, M., Houze, R. A., Jr, & Yuter, S. E. (1995). Climatological characterization of three-dimensional storm structure from operational radar and rain gauge data. *Journal of Applied Meteorology*, *34*(9), 1978–2007.

Sun, J. (2005). Initialization and numerical forecasting of a supercell storm observed during STEPS. *Monthly Weather Review*, *133*(4), 793–813.

Ulbrich, C. W. (1983). Natural variations in the analytical form of the raindrop size distribution. *Journal of Climate and Applied Meteorology*, *22*(10), 1764–1775.

Vivekanandan, J., Ellis, S., Oye, R., Zrnic, D., Ryzhkov, A., & Straka, J. (1999). Cloud microphysics retrieval using S-band dual-polarization radar measurements. *Bulletin of the American Meteorological Society*, *80*(3), 381–388.

Vivekanandan, J., Zhang, G., & Brandes, E. (2004). Polarimetric radar estimators based on a constrained gamma drop size distribution model. *Journal of Applied Meteorology*, *43*(2), 217–230.

Wang, M., Zhao, K., Xue, M., Zhang, G., Liu, S., Wen, L., & Chen, G. (2016). Precipitation microphysics characteristics of a Typhoon Matmo (2014) rainband after landfall over eastern China based on polarimetric radar observations. *Journal of Geophysical Research: Atmospheres*, *121*(20), 12415–12433. https://doi.org/10.1002/2016JD025307

Waterman, P. C. (1965). Matrix formulation of electromagnetic scattering. *Proceedings of the IEEE*, *53*(8), 805–812.

Wen, L., Zhao, K., Chen, G., Wang, M., Zhou, B., Huang, H., et al. (2018). Drop size distribution characteristics of seven typhoons in China. *Journal of Geophysical Research: Atmospheres*, *123*(12), 6529–6548. https://doi.org/10.1029/2017JD027950

Wen, J., Zhao, K., Huang, H., Zhou, B., Yang, Z., Chen, G., et al. (2017). Evolution of microphysical structure of a subtropical squall line observed by a polarimetric radar and a disdrometer during OPACC in Eastern China. *Journal of Geophysical Research: Atmospheres*, *122*(15), 8033–8050. https://doi.org/10.1002/2016JD026346

Wen, L., Zhao, K., Wang, M., & Zhang, G. (2019). Seasonal variations of observed raindrop size distribution in East China. *Advances in Atmospheric Sciences*, *36*(4), 346–362. https://doi.org/10.1007/s00376-018-8107-5

Wen, L., Zhao, K., Zhang, G., Liu, S., & Chen, G. (2017). Impacts of instrument limitations on estimated raindrop size distribution, radar parameters, and model microphysics during Mei-Yu season in East China. *Journal of Atmospheric and Oceanic Technology*, *34*(5), 1021–1037. https://doi.org/10.1175/JTECH-D-16-0225.1

Wen, L., Zhao, K., Zhang, G., Xue, M., Liu, S., Bowen, Z., & Chen, X. (2016). Statistical characteristics of raindrop size distributions observed in East China during the Asian summer monsoon season using 2D-video disdrometer and Micro-rain radar data. *Journal of Geophysical Research: Atmospheres*, *121*(5), 2265–2282. https://doi.org/10.1002/2015JD024160

Xu, W. (2013). Precipitation and convective characteristics of summer deep convection over East Asia observed by TRMM. *Monthly Weather Review*, *141*(5), 1577–1592.

Xue, M. (2016). Preface to the special issue on the "Observation, Prediction and Analysis of Severe Convection of China" (OPACC) National "973" Project. *Advances in Atmospheric Sciences*, *33*(10), 1099–1101.

Yang, Z., Zhao, K., Xu, K., Li, K., Chen, G., Wen, L., et al. (2019). Microphysical characteristics of extreme convective precipitation over Yangtze-Huaihe River Basin during Meiyu season using polarimetric radar data (in Chinese). *Acta Meteorologica Sinica*, *77*(1), 58–72.

Yuter, S. E., & Houze, R. A., Jr (1995). Three-dimensional kinematic and microphysical evolution of Florida cumulonimbus. Part II: Frequency distributions of vertical velocity, reflectivity, and differential reflectivity. *Monthly Weather Review*, *123*(7), 1941–1963.

Zhang, G. (2015). Comments on "Describing the shape of raindrop size distributions using uncorrelated raindrop mass spectrum parameters". *Journal of Applied Meteorology and Climatology*, *54*(9), 1970–1976.

Zhang, G. (2016). *Weather radar polarimetry*. CRC Press.

Zhang, G., Sun, J., & Brandes, E. A. (2006). Improving parameterization of rain microphysics with disdrometer and radar observations. *Journal of the Atmospheric Sciences*, *63*(4), 1273–1290.

Zhang, C.-Z., Uyeda, H., Yamada, H., Geng, B., & Ni, Y. (2006). Characteristics of mesoscale convective systems over the east part of continental China during the Meiyu from 2001 to 2003. *Journal of the Meteorological Society of Japan*, *84*(4), 763–782.

Zhang, G., Vivekanandan, J., & Brandes, E. (2001). A method for estimating rain rate and drop size distribution from polarimetric radar measurements. *IEEE Transactions on Geoscience and Remote Sensing*, *39*(4), 830–841.

Zhang, G., Vivekanandan, J., Brandes, E. A., Meneghini, R., & Kozu, T. (2003). The shape-slope relation in observed gamma raindrop size distributions: Statistical error or useful information?. *Journal of Atmospheric and Oceanic Technology*, *20*(8), 1106–1119.